energies

MDPI

Article

Density Functional Theory-Based Molecular Modeling: Verification of Decisive Roles of Van der Waals Aggregation of Triiodide Ions for Effective Electron Transfer in Wet-Type N3-Dye-Sensitized Solar Cells

Susumu Yanagisawa [1,*] and Shozo Yanagida [2,*]

[1] Department of Physics and Earth Sciences, Faculty of Science, University of the Ryukyus, Senbaru, Nishihara, Okinawa 903-0213, Japan
[2] M3 Laboratory, Inc., Osaka University, ISIR, 8-2, Ibaraki, Osaka 567-0047, Japan
* Correspondence: shou@sci.u-ryukyu.ac.jp (S.Y.); yanagida@mls.eng.osaka-u.ac.jp (S.Y.)

Received: 18 May 2020; Accepted: 5 June 2020; Published: 11 June 2020

Abstract: Density functional theory-based molecular modeling (DFT/MM) validates that KI and I_2 undergo exothermic van der Waals (vdW) aggregation in acetonitrile (AN) or in the presence of 4-tert-butylpyridine (TBP), forming potassium triiodide (KI_3) and, further mutual vdW aggregation leads to the formation of $(KI_3)_2$ and AN, $(KI_3)_2$ and $(AN)_2$ and $(KI_3)_2$ and TBP in the AN-based Dye sensitized solar cells (DSSC) electrolytes. All KI_3 aggregates have a very low energy gap, 0.17 eV, 0.14 eV and 0.05 eV of lowest unoccupied molecular orbital (LUMO) + 1 and LUMO, respectively, verifying efficient electron diffusion in μm-thick DSSC electrolytes. Hydrogen-bonding aggregation of anatase TiO_2 model, $Ti_9O_{18}H$ and OH, with N3 (proton) dye is also validated by DFT/MM, and the energy structure verifies unidirectional electron flow from highest occupied molecular orbital (HOMO) on thiocyanide (SCN) groups of N3 dye to LUMO on the TiO_2 model at the aggregates. Further, DFT/MM for the aggregation of $K^+I_3^-$ with N3 verifies the most exothermic formation of the aggregate of N3 (proton) and $K^+I_3^-$. The UV-Vis spectra of N3 (proton) and $K^+I_3^-$ is consistent with reported incident photocurrent efficiency (IPCE) action spectra (λ = 450–800 nm) of N3-sensitized DSSC, verifying that the N3 dye of N3 (proton) and $K^+I_3^-$ becomes an effective sensitizer in the anode / TiO_2 / N3 (proton) / KI/I_2 / acetonitrile (AN) / cathode structured DSSC. The energy structure of LUMO and LUMO + 1 of the aggregates, $Ti_9O_{18}H$ and OH and N3 (proton), N3 and $K^+I_3^-$, $(KI_3)_2$ and AN and $(KI_3)_2$ and TBP verifies high IPCE photocurrent and effective electron diffusion via KI_3-aggregates in the DSSC of $Ti_9O_{18}H$ and OH and N3 (proton) and $K^+I_3^-$.

Keywords: density functional theory; van der Waals Coulomb interactions; triiodide ion; electrostatic potential map

1. Introduction

As reported in the preceding papers [1–6], quantum chemistry molecular modeling, i.e., density functional theory-based molecular modeling (DFT/MM) can be regarded as theory-based "experiments". DFT/MM can be carried out very quickly using high-end supercomputer-like personal computers. DFT/MM are applicable to molecular aggregates which are induced by van der Waals (vdW) force (including hydrogen bonding and Coulomb interactions). DFT/MM for the structuring of aggregates gives the heat of formation, dipole moment for understanding solubility in polar solvent like water and acetonitrile (AN) and the energy structures of aggregates, i.e., surface orbital electron energy structures [almost degenerate highest molecular orbitals [HOMO (n), n = 0–4)] and the lowest unoccupied molecular orbitals [LUMO + n, n = 0–2)]. Their molecular orbital configurations are

evaluated as theory-based "experimental" data for verification and prediction of interacting molecules. Semiconducting property of the aggregates can be verified by the orbital energy gap between LUMO and LUMO + 1 [2,3]. We performed DFT/MM using the B3LYP exchange correlation functional and the 6–31G(d) basis set with Spartan'18 (Wavefunction, Inc. Irvine, CA). Prior to the DFT calculation for electronic properties, the geometries of the molecular aggregates were determined by the molecular mechanics employing the Merck molecular force field (MMFF).

Since the first report of its high-performance by O'Regan and Grätzel [7], the dye-sensitized solar cell (DSSC) using KI / I_2 / acetonitrile electrolyte has been a focus for a fundamental understanding of microscopic electronic phenomena of TiO_2, dye molecules and electrolytes [8]. As for wet-type DSSC electrolytes of acetonitrile (AN), KI and I_2, redox couple of $I^-/I_3^-$was introduced to explain electron diffusion by electron hopping and exchange mechanisms [9]. Recently, we reported that DFT/MM verifies the semiconducting properties for quasi-solid state $I_5^-N(CH_3)_4^+$ -based electrolytes of DSSC [1]. In addition, we clarified that $PbI_6^{4-}/MeNH_3^+$ -based perovskite solar cells have excellent electron diffusion among panchromatic $PbI_6^{4-}/MeNH_3^+$ matrixes in the solar cells [2,3]. We have ascribed excellence of perovskite solar cells to $PbI_6^{4-}/MeNH_3^+$ -induced vdW aggregation. Here, we corroborate that the iodine element-based vdW aggregations also play an important role in unidirectional electron diffusion in wet-type DSSC using KI/I_2/acetonitrile electrolytes.

2. Results

2.1. DFT-Based Electrostatic Potential Map (EPM) and Van der Waals Aggregation

Figure 1 shows the EPM of I_2, KI, and AN.

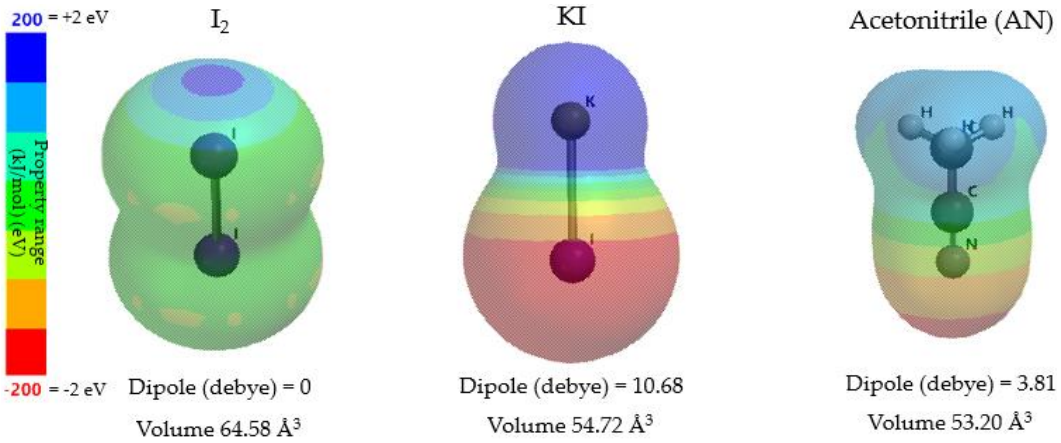

Figure 1. Electrostatic potential map with dipole as a measure of solubility: (**a**) I_2; (**b**) KI; (**c**) acetonitrile (AN).

In the colorful electrostatic potential map (ESPM), the property range (kJ/mol, eV) indicates potential energy of surface electron density of molecules and of vdW aggregates. Blue surface color is particularly electron poor and subject to electrophilic attack (electron poor vdW surface), and red surface color is particularly electron rich, subject to nucleophilic attack (electron rich vdW surface). As quantitative structured activity, volume (Å^3) of molecules is determined by the CPK model, reflecting surface electron number of molecules and aggregates. It may be added that the blue region corresponds to the LUMO rich region, and the red region to the HOMO rich region.

Pale blue EPM of I_2 indicates its electrophilic nature and the top surface is particularly electrophilic. Colorful EPM of KI and AN indicate the presence of both electrophilic and nucleophilic surface, reflecting large dipole, 10.68 debye and 3.81 debye, respectively. It is worth noting that the volumes of I_2 and

KI are much larger than that of AN. Van der Waals aggregation occurs between electrophilic electron surface and nucleophilic one.

2.2. Verification of KI_3 Formation by Van der Waals Aggregation of I_2 and KI in Electrolytes

We speculate that the minimum number of molecules which may form vdW aggregates in AN should be three, and one of them is AN. Figure 2 shows ESPM of equilibrium geometry of vdW aggregates of $(I_2)_2$AN, $(KI)_2$AN, and acetonitrile $(AN)_3$. When compared to ESPM of I_2, and KI and AN in Figure 1, all of trimeric aggregates result from vdW aggregation between the electron-poor electrophilic surface and the electro-rich nucleophilic surface.

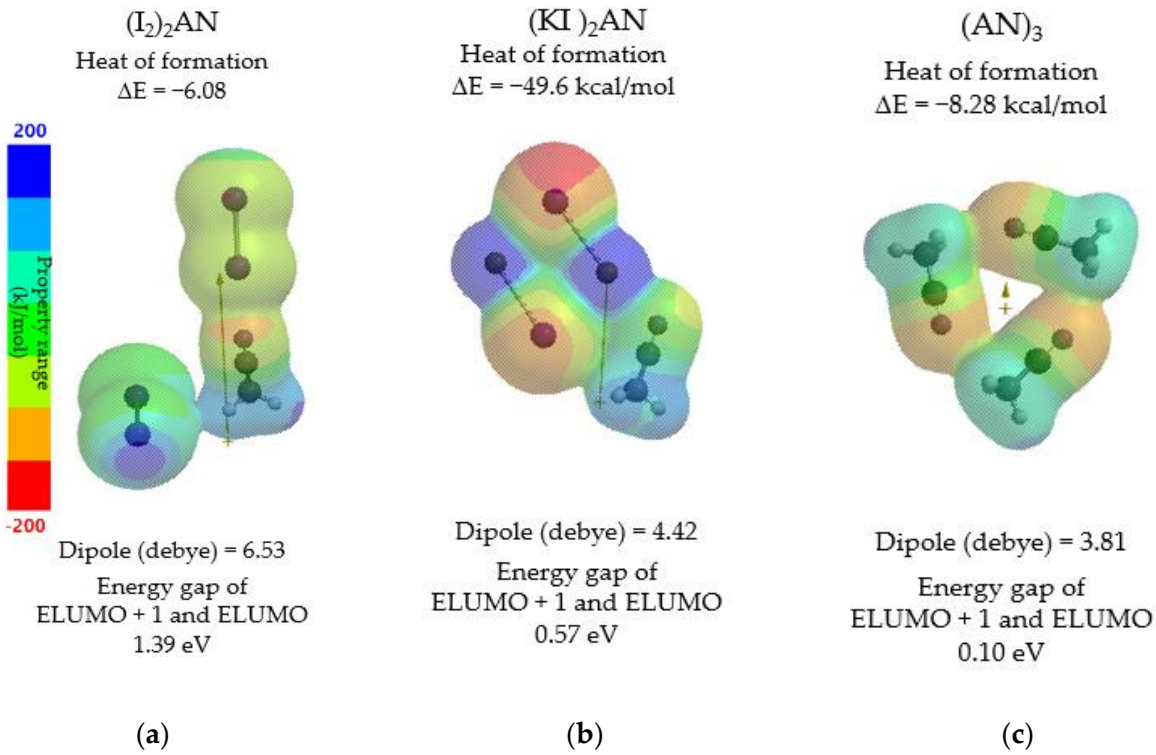

Figure 2. Electrostatic potential map (ESPM) with the heat of formation, dipole as measure of solubility and energy gap of energy of lowest unoccupied molecular orbital (ELUMO) + 1 and ELUMO as measure of conductivity: (**a**) $(I_2)_2$AN; (**b**) $(KI)_2$AN; (**c**) acetonitrile $(AN)_3$.

All vdW aggregates form exothermically, suggesting stability in AN. The most stable vdW aggregate of $(KI)_2$AN (heat of formation is −49.6 kcal/mol) gives a colorful ESPM, predicting further vdW aggregation with KI and I_2 in AN.

Figure 3 shows ESPM of I_2 and KI and AN, KI_3 and I_2 and KI, and KI_3 and $(AN)_2$. All vdW aggregates give large heat of formation and, interestingly, I_2 aggregates with KI in aggregate of I_2 and KI and AN. Geometry of I_3^- gives angle of 172° comparable to that of geometry I_3^- in KI_3 and $(AN)_2$. DFT/MM-determined UV-Vis spectrum comparison (λmax: 447 nm and 414 nm) verifies in situ formation of KI_3 from I_2 and KI in AN. In situ formation of KI_3 from I_2 and KI is also confirmed in vdW aggregate of KI_3 and I_2 and KI.

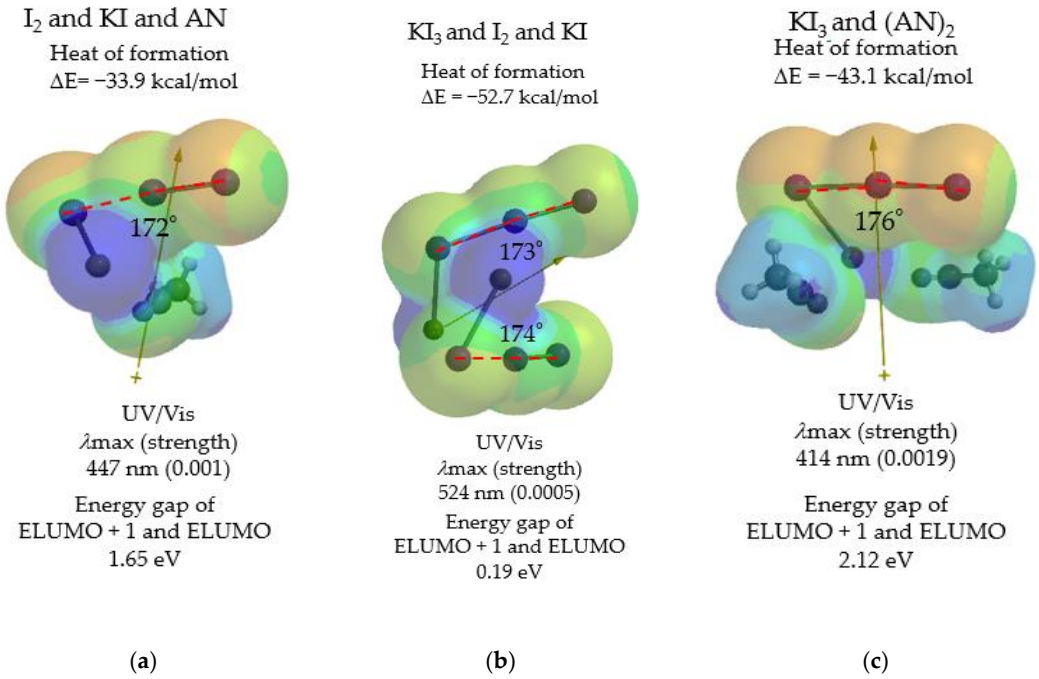

Figure 3. Equilibrium geometry of van der Waals aggregates and their heat of formation and Electrostatic potential map (ESPM) of energy structures: (**a**) I_2 and KI and AN; (**b**) KI_3 and I_2 and KI; (**c**) KI_3 and $(AN)_2$.

2.3. Van der Waals Aggregation of Potassium Triiodide (KI_3) and 4-Tertbyutylpyridine (TB) Effect on DSSC Electrolytes

Interestingly, DFT/MM of vdW aggregate of KI_3 and I_2 and KI reveals that the energy gap of ELUMO + 1 and ELUMO is 0.19 eV, predicting that the aggregate is semiconducting once it is formed. With this prediction in mind, DFT/MM is extended to vdW aggregates of $(KI_3)_2$ and AN, and of $(KI_3)_2$ and $(AN)_2$ to clarify the reason why the electrolyte of KI /I_2 /AN become semiconducting. In addition, since it is well-known that presence of 4-tert-butylpyridine (TBP) in the electrolytes improves open circuit voltage (Voc) of DSSC. Open circuit voltage depends on electron leak-free unidirectional photocurrent [8,10]. DFT/MM is also extended to vdW aggregate of $(KI_3)_2$ and TBP.

Figure 4 shows the EPSM of equilibrium geometry of vdW aggregates of $(KI_3)_2$ and AN, $(KI_3)_2$ and $(AN)_2$, $(KI_3)_2$ and TBP. The heat of formation values verify exclusive formation of vdW dimer of KI_3 in wet type DSSC electrolytes. UV-Vis spectra support the orange color of the electrolytes. Energy gaps of LUMO + 1 and LUMO are all less than 0.2 eV, and their configurations explain unidirectional electron flow from LUMO + 1 to LUMO. Interestingly, the vdW aggregate of $(KI_3)_2$ and TBP gives the smallest energy gap of 0.05 eV.

In order to validate conductivity of electron-running state of the vdW aggregates of KI_3 -based electrolytes, EPM and energy structures of electron injected $[(KI_3)_2$ and $AN]^{\cdot -}$ and $[(KI_3)_2$ and $TBP]^{\cdot -}$ are examined (Figure 5). Reddish ESPM indicates nucleophilic surface state, both negative values of heat of their electron acceptance verify their electron acceptability, and hopping between them is favorable in the electrolytes. As for surface energy structures, Ea (HOMO) is identical with electron singly occupied molecular orbital (SOMO). Accepted electron (spin density) is located in bLUMO. We understand that spin may run on bLUMO at electron running process. The energy gap of bLUMO and SOMO (0.46 eV and 0.35 eV, respectively), is small enough for spin (unpaired electron) to run under irradiance of solar energy ($h\nu$).

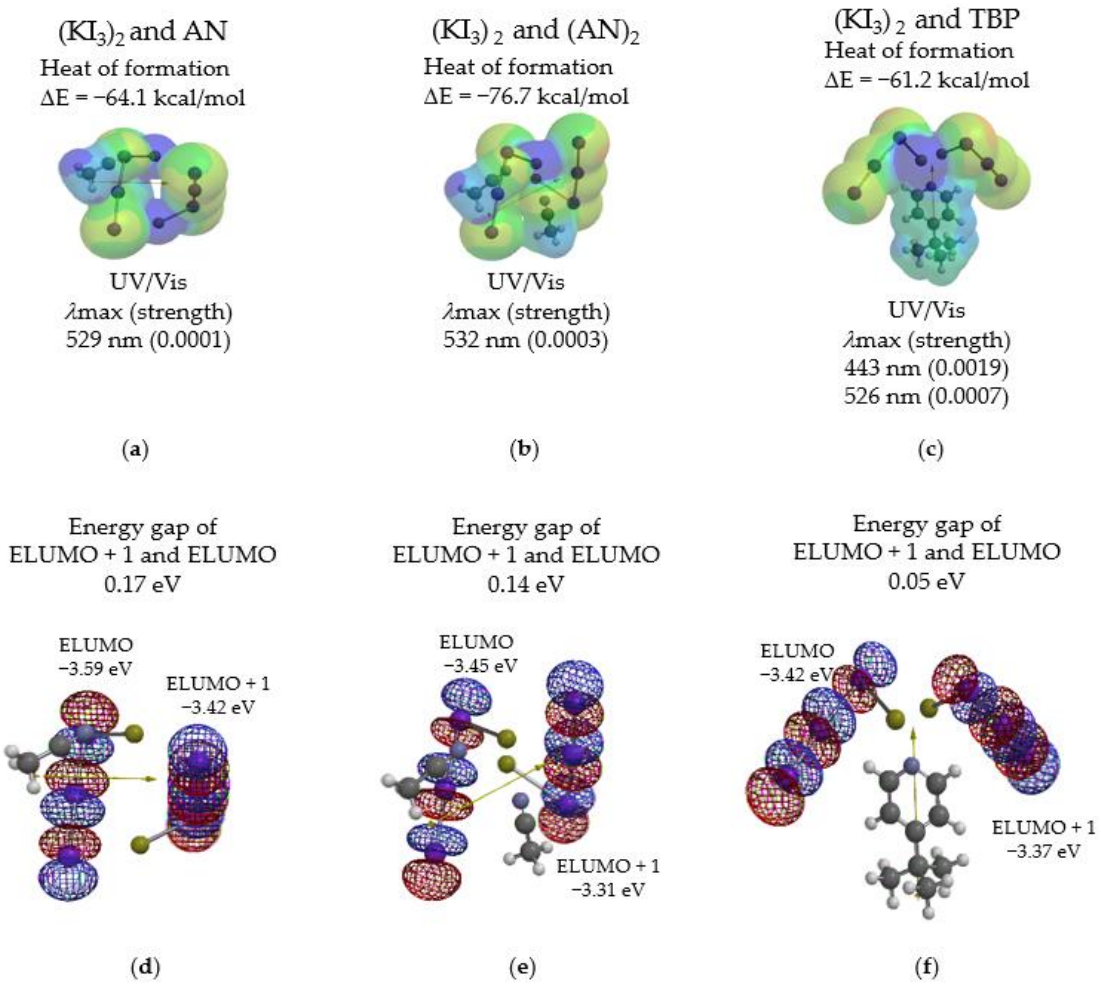

Figure 4. Equilibrium geometry of van der Waals aggregates, heat of formation and energy gap of ELUMO + 1 and ELUMO: (**a**) $(KI_3)_2$ and AN; ΔE = −64.1 kcal/mol (**b**) $(KI_3)_2$ and $(AN)_2$; (**c**) $(KI_3)_2$ and 4-tert-butylpyridine (TBP); (**d**) LUMO configuration of $(KI_3)_2$ and AN; (**e**) LUMO configuration of $(KI_3)_2$ and $(AN)_2$; (**f**) LUMO configuration of $(KI_3)_2$ and 4-tert-butylpyridine (TBP).

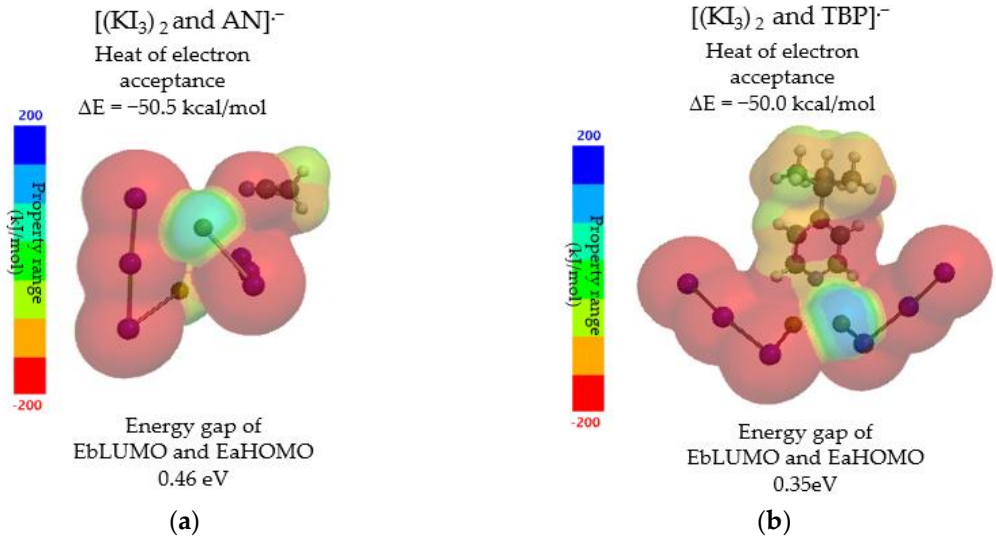

Figure 5. *Cont.*

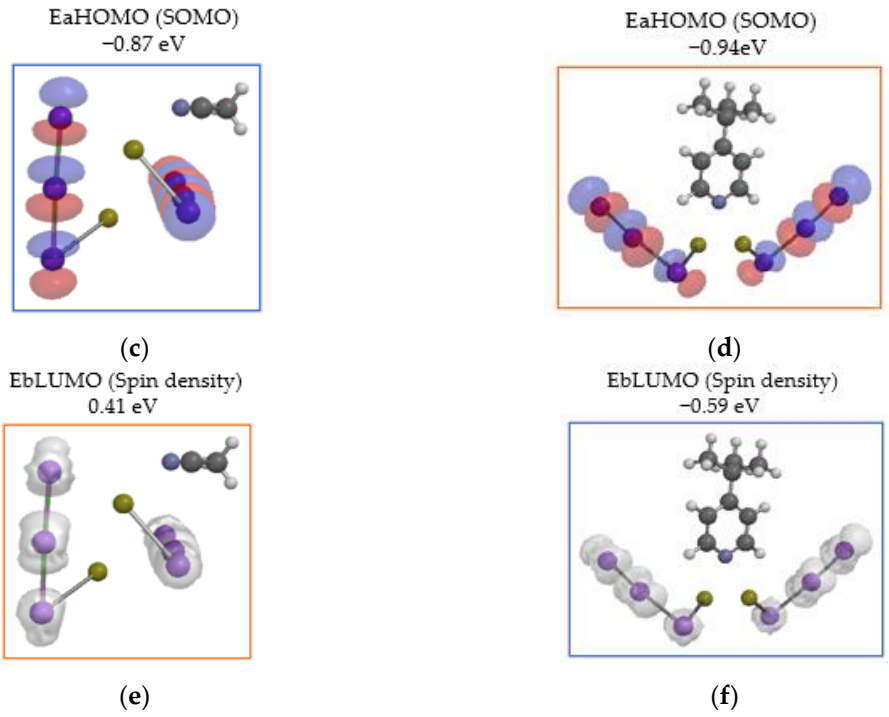

Figure 5. Equilibrium geometry of electron running-state with heat of electron acceptance and energy structures: (**a**) ESPM of $[(KI_3)_2$ and AN$]^{\cdot-}$; (**b**) ESPM of $[(KI_3)_2$ and TBP$]^{\cdot-}$; (**c**) SOMO configuration of $[(KI_3)_2$ and AN$]^{\cdot-}$; (**d**) EbLUMO configuration of $[(KI_3)_2$ and TBP$]^{\cdot-}$; (**e**) EbLUMO configuration of $[(KI_3)_2$ and AN$]^{\cdot-}$; (**f**) $[(KI_3)_2$ and TBP$]^{\cdot-}$.

2.4. Electrostatic Potential Map (ESPM) of TiO_2 Anatase Nanoparticle and Conductivity

Figure 6 shows the ESPM of anatase TiO_2 model of $Ti_9O_{18}H$ and OH proposed by Jono and Yamashita (Jono-Yamashita model) [11]. The validity of the Jono-Yamashita model for TiO_2 nanoparticle (NP) has been confirmed elsewhere [12]. Colorful ESPM verifies that three-dimensional vdW aggregates may form TiO_2 thin films and result in giving porous structures when sintered at high temperature.

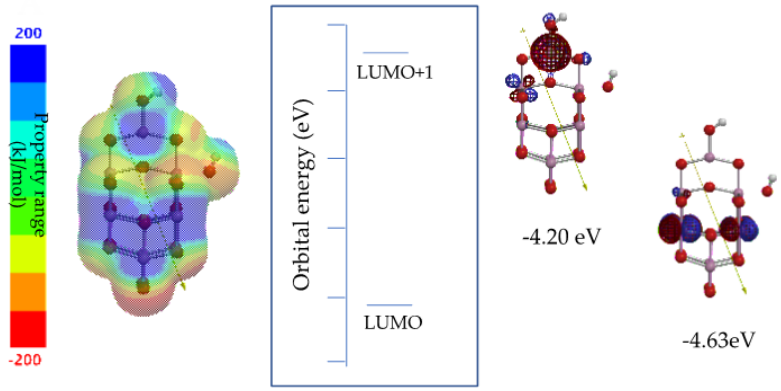

(**a**)

Figure 6. *Cont.*

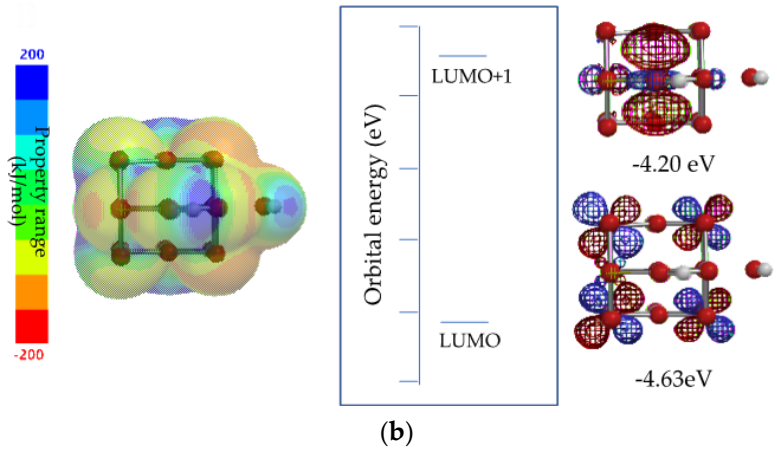

Figure 6. Electrostatic potential map and electron energy structure of TiO_2 anatase model of $Ti_9O_{18}H$ and OH: (**a**) side view; (**b**) view from top.

To understand the nature of electron acceptability and electron-transfer in TiO_2, electron running molecular orbital configurations of LUMO and LUMO + 1 are shown as the side view (a) and the view from the top (b) of the TiO_2 model. The energy gap of LUMO + 1 and LUMO is 0.43 eV, which verifies and predicts that TiO_2 model and their vdW aggregates become semiconducting when LUMO and LUMO + 1 accept photoelectron.

2.5. Electrostatic Potential Map (ESPM) of Sensitizing N3 Dyes and Perspective of Van der Waals Aggregation

Figure 7 shows ESPM of two kinds of N3 (tetramethylammonium) (a homolog of N719) and N3 (proton) with UV-Vis spectra and electron energy structures. Colorful ESPM suggests that they are likely not to aggregate each other, but orange-colored SCN group sites may be vdW-aggregated by electrophilic potassium triiodide ($K^+I_3^-$). Each energy gap of LUMO + 1 and LUMO, 0.36 eV and 0.10 eV predicts that both N3 dyes are conductive.

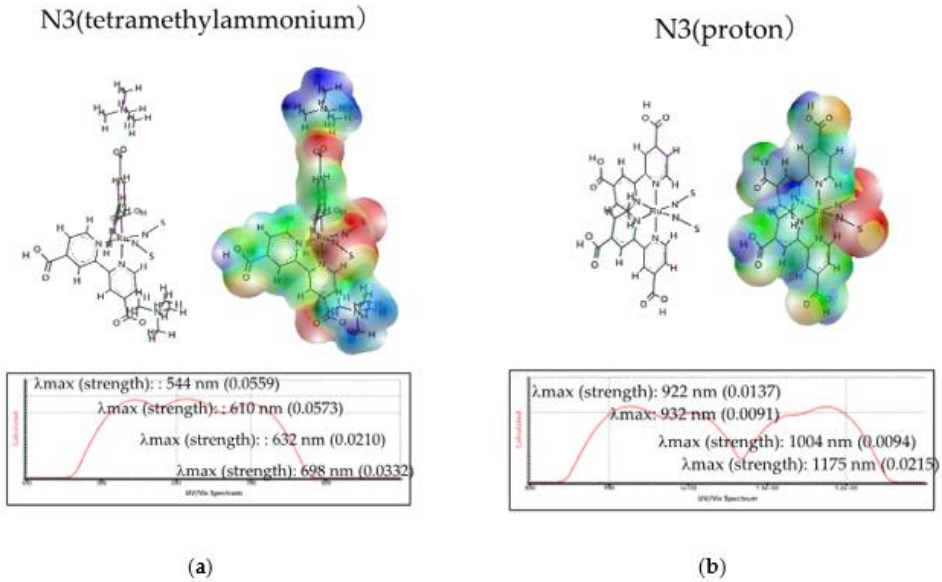

Figure 7. Electrostatic potential map and energy structures of N3 dyes: (**a**) N3 (tetramethylammonium); (**b**) N3 (proton).

Recently we reported that DFT/MM predict that DFT/MM-determined UV-Vis absorption spectra are strongly affected by vdW aggregation with other molecules, which was exemplified by UV-Vis spectrum of benzene solution [3]. Figure 7 reveals that DFT/MM-based UV-Vis spectrum of N3

(tetramethylammonium) is quite comparable to the incident photocurrent efficiency (IPCE) action spectra of N3-sensitized DSSC [13]. However, UV-Vis spectrum of N3 (proton) gives 380 nm red shifted one with decreased strength of absorption. DFT/MM-determined three-dimensional molecular structures verify that the difference comes from a change of coordination structure of ligands, bipyridyl and SCN ligands around Ru(II) ion (see Section 3).

2.6. Verification of Van der Waals Aggregation of N3 Dye with Anatase TiO_2 Model

Here, let us consider vdW aggregation of anatase TiO_2 and N3 dye molecule, which may allow us to gain insights into the electronic natures of the TiO_2 /N3 (proton) dye interface in DSSC. The problem of dye-anchoring on anatase TiO_2 had been argued several times in the past, e.g., ester formation with bipyridyl carboxylic acid ligand (bpy-dca), coordination of the bipyridyl ligand to Ti(IV), and hydrogen bonding with the bipyridyl ligand [14–16]. DFT/MM now verifies that N3 dye can be anchored by van der Waals force of hydrogen bonding between the hydroxyl group on TiO_2 and the carboxyl group of N3 dye (Figure 8). Heat of formation of −13.1 kcal/mol is not large enough to form strong vdW aggregation. We failed to obtain UV-Vis absorption spectra of the aggregate. However, surface electron energy structures, EHOMO and ELUMO and their configurations verify that photoexcitation of N3 dye induces electron injection from HOMO's on SCN ligands to LUMO's on anatase TiO_2.

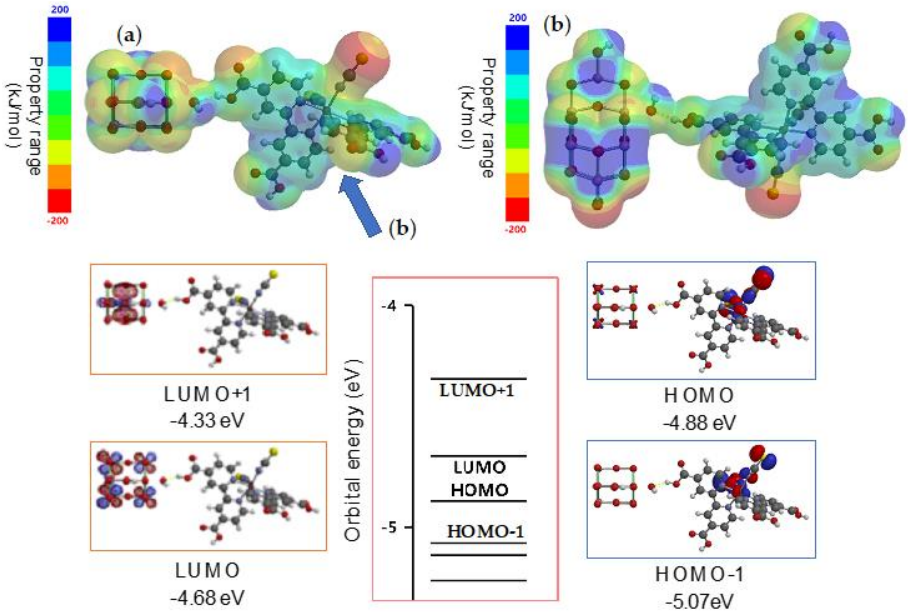

Figure 8. Electrostatic potential map (ESPM) of N3 (proton), adsorbed TiO_2 anatase model of $Ti_9O_{18}H$ and OH and N3 (proton) and electron energy structures with HOMO/LUMO configuration for (**a**): (**a**) view from top; (**b**) side view.

2.7. Van der Waals Aggregation of N3 Dye with Potassium Triiodide

Remarkable vdW aggregation power of in situ formed potassium triiodide works on N3 (proton) dye molecules (Figure 9). Formation of vdW-aggregate of N3 (proton) and $(KI_3)_2$ and of N3(proton) and $K^+I_3^-$ are both exothermic ($\Delta E = -79.7$ kcal/mol and $\Delta E = -142$ kcal/mol respectively) and UV-Vis absorption maxima shift from near IR region to visible region. Interestingly, the UV-Vis spectra of the KI aggregates are consistent with reported IPCE action spectra (λ = 600–700 nm) of N3-sensitized DSSC [13].

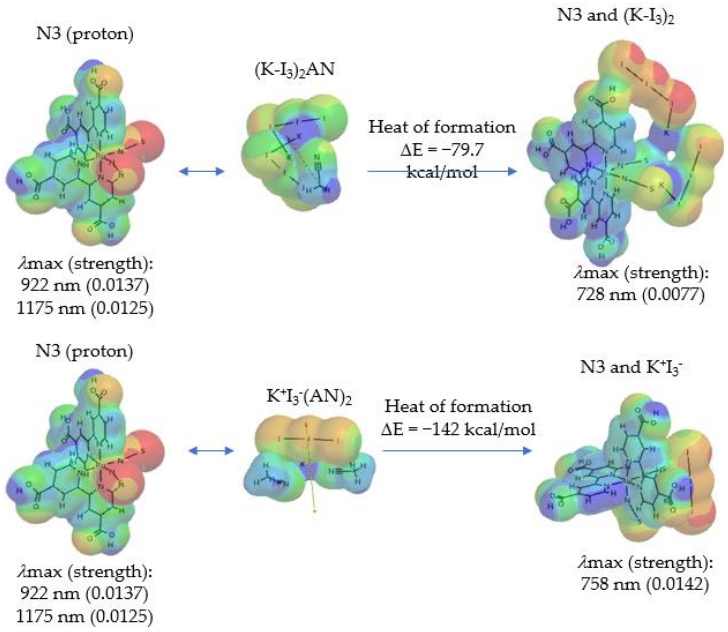

Figure 9. Van der Waals Aggregation of N3 with potassium triiodide to respective N3 and $(KI_3)_2$ and N3 and $K^+I_3^-$.

The most stabilized vdW aggregate of N3 (proton) and $K^+I_3^-$ can be regarded as a new type of triiodide aggregated ruthenium dye. DFT/MM assigns the absorption maximum to molecular orbital components. All of them are regarded as results of photoexcitation from HOMO's on SCN ligands to LUMO's on bipyridyl ligands (Figure 10).

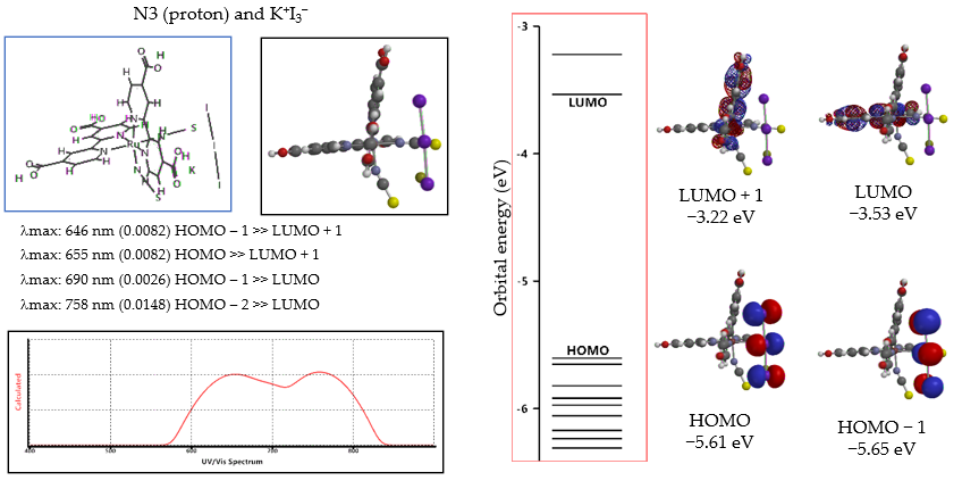

Figure 10. Energy structure of van der Waals (vdW)-aggregate of N3 (proton) with potassium triiodide of N3 (proton) and $K^+I_3^-$. UV-Vis spectrum and surface electron energy structure.

3. Discussion

Photoconversion efficiency (η) of solar cells of DSSC is determined by the following Equation:

$$\eta = J_{sc} \times V_{oc} \times ff \,/\, E \tag{1}$$

where J_{sc} is the short circuit photocurrent, V_{oc} is the open circuit voltage, ff is fill factor and E is solar energy 100 mW/cm^2.

Nazeeruddin, who invented a series of N3 dyes, reported that N3-dye-sensitized DSSC give J_{sc} = 16.8–19.0 mA/cm^2, V_{oc} = 600–770 mV, and ff 0.65–0.72, and photoconversion efficiency (η) at

AM 1.5, 7.4–9.3%. In addition, he successfully measured excellent IPCE spectra (λ = 500–630 nm (70–80%)) of DSSC sensitized by respective N3 (proton) and N3 (tetrabutylammonium) (N719) [13].

In Figure 11, DSSC key components, anatase TiO_2 model, in situ-formed I_3^- -aggregated N3 dye of N3 and $K^+I_3^-$, KI_3-dimer aggregates, $(KI_3)_2$ and AN, and $(KI_3)_2$ and TBP, are aligned referring to the electrostatic potential map (ESPM). The pale green colored ESPM of $(KI_3)_2$ and AN, and $(KI_3)_2$ and TBP predict further vdW aggregation. Especially, vdW aggregation between N3 and $K^+I_3^-$, and $(KI_3)_2$ and AN or $(KI_3)_2$ and TBP is apparent in view of ESPM.

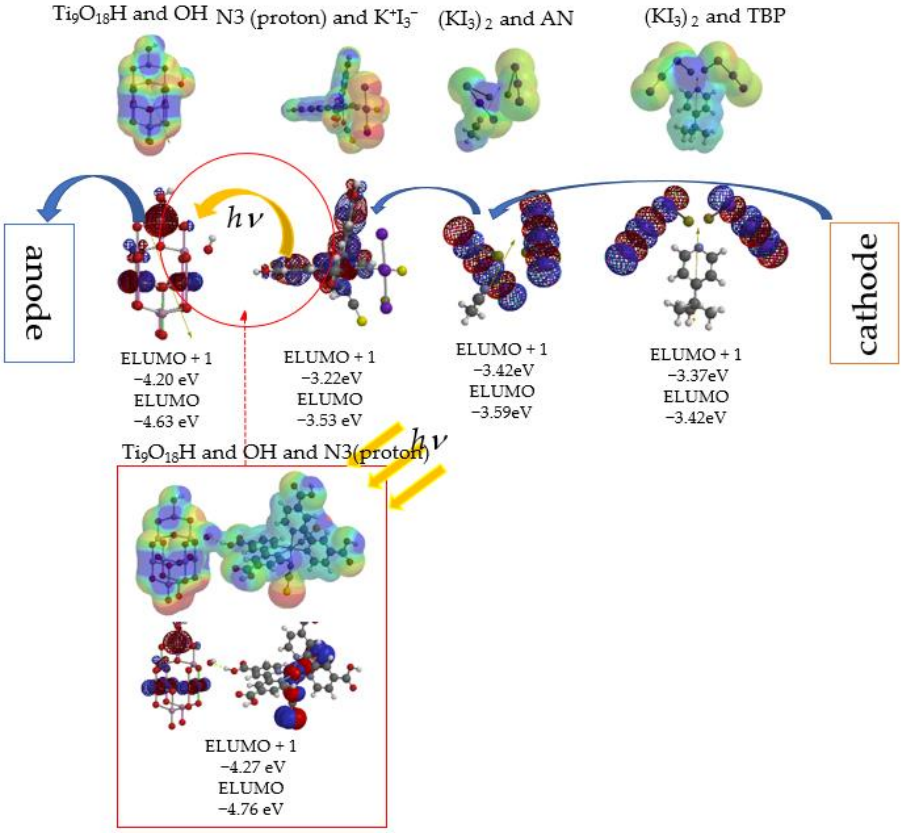

Figure 11. Visualization of unidirectional electron diffusion via vdW aggregation in DSSC composed of $Ti_9O_{18}H$ and OH/N3 (proton) /KI_3 in acetonitrile (AN).

The above-mentioned high V_{oc} = 0.6–0.77 mV and the fill factors 0.65–0.72 of DSSC are validated as follows: Photo-formed electron runs through degenerate LUMO and LUMO + 1. Each LUMO + 1 and LUMO configuration visualize effective electron transfer in DSSC devices by following comparable potential energy of the KI_3-assisted aggregates (Figure 11).

Photoelectron on irradiated $Ti_9O_{18}H$ and OH and N3 (proton) has a potential from −3.22 eV to −3.53 eV and transfer to LUMO + 1 and LUMO with potential from −4.20 eV to −4.63 eV. Photoelectron may have potential energy of 0.98–1.1 eV on anode to cathode. In general, clear-cut V_{oc} becomes measurable by effective electron transfer via electrolytes of $(KI_3)_2$ and AN, and of $(KI_3)_2$ and TBP. The measured V_{oc} = 0.6–0.77 mV is less than theoretical ones of 0.98–1.1 eV, and means that photoelectron leakage is not suppressed enough on N3-anchored TiO_2 NP electrodes. Improved conductivity of $(KI_3)_2$ and TBP (energy gap: 0.05 eV) is consistent with enhancement of conversion efficiency of solar cells.

The IPCE action spectrum ranges are 350–800 nm; at 350 nm (about 50%), at 500–630 nm (70–80%) and at 800 nm (about 5%) [13]. The excellent IPCE action spectra for N3-sensitized DSSC is now validated theoretically due to effective visible light-absorption of N3 and K^+I^- dyes on porous TiO_2 films.

Figure 12 shows a comparison of the UV-Vis spectra of N3 (proton), N3 and $K^+I_3^-$, and N3 (tetramethylammonium) as a homologue of N719. UV-Vis allowed transition occurs between highest occupied molecular orbital (HOMO), HOMO − 1, and HOMO − 2 on SCN ligands to lowest unoccupied molecular orbital (LUMO), LUMO + 1, and LUMO + 2 on bpy-dca ligands. In addition, when the molecular structures are compared, the coordination structures of N3 and $K^+I_3^-$ and N3 (tetramethylammonium) are quite comparable, explaining that the respective 280 nm and 380 nm blue shift (bathochromic shift) comes from ligand-coordination change induced by vdW and Coulomb interaction of N3 with I_3^- and tetramethylammonium. The hyperchromic effect of increase of strength (ε) and the bathochromic effect (the red shift) in absorption spectrum of N3 (tetramethylammonium) validates that N719 is a respectable sensitizer of DSSC.

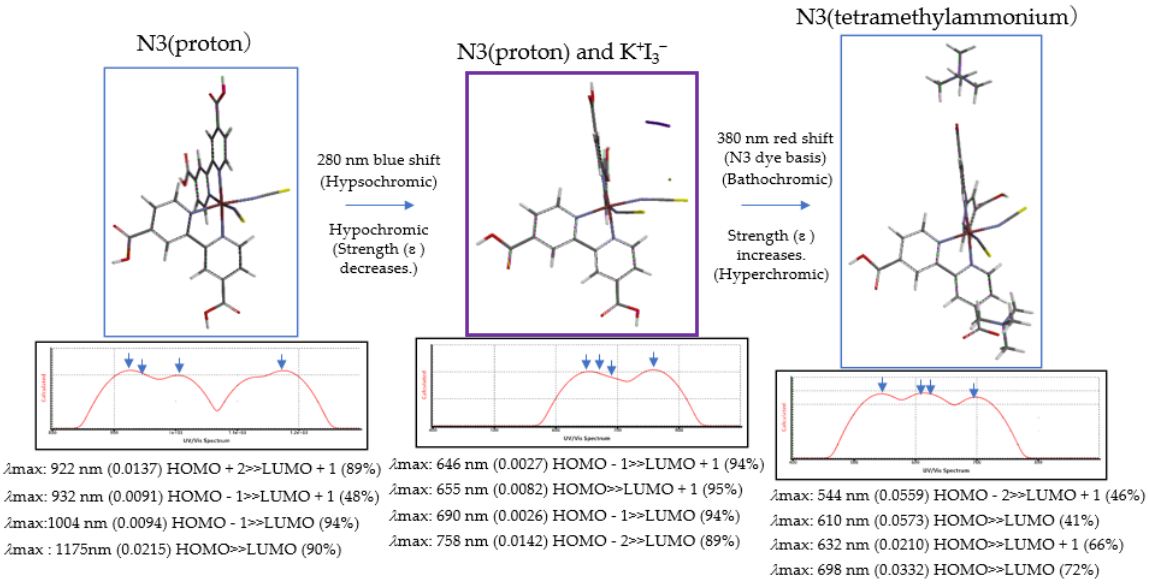

N3 dye	HOMO eV	HOMO - 1 eV	HOMO - 2 eV	LUMO eV	LUMO + 1 eV	Energy gap of LUMO + 1 and LUMO eV
N3 and $(K^+I_3^-)_2$	−5.01	−5.65	−5.82	−3.53	−3.22	0.31
N3 (tetramethylammonium)	−4.76	−4.97	−4.98	−2.44	−2.08	0.32
N3(proton)	−4.82	−4.98	−5.04	−3.22	−3.12	0.10

Figure 12. Comparison of DFT/MM-predicted UV-Vis spectra and energy structures of TiO_2 sensitizing dyes of N3 (proton), N3 (proton) and $K^+I_3^-$ and N3 (tetramethylammonium).

4. Conclusions

Experimental and theoretical UV-Vis spectral analyses of sensitizing dyes on TiO_2 NPs were not successful enough so far [17–20]. As we reported [3,5], Spartan (Q-Chem) (Wavefunction, Inc. Irvin. CA, USA) is a comprehensive *ab-initio* quantum-chemistry software for accurate predictions of molecular structures, reactivities, and vibrational, electronic and NMR spectra. We are very proud of the verification power of density functional theory-based molecular modeling (DFT/MM) using Spartan (involving Q-Chem), and now demonstrate that vdW aggregation power of triiodide ion contributes to solar light harvesting of N3 and effective electron diffusion in in situ formed triiodide ion-based electrolytes. The strong tendency of vdW aggregation via I_3^- at interfaces of DSSC facilitates DSSC fabrication with high performance of fill factor (*ff*) and respectable open circuit voltage (V_{oc}).

As a perspective conclusion, DFT/MM is a useful tool for verifying and predicting conductivity of electronic molecular aggregates, IPCE action spectra and theoretical V_{oc} of solar cells, as mentioned in the DFT/MM of perovskite solar cells [3].

During editing period of the article, we succeeded to obtain DFT/MM-based UV-Vis spectrum of van der Waals aggregate of N3(proton) with two acetonitrile (AN) molecules (see Supplementary).

It is now verified that the aggregation of N3 with AN, i.e. solvation of AN to N3, also affect energy structures of N3, giving four λmax: 692 nm (0.0008), 823 nm (0.0242), 875 nm (0.0164), 875 nm (0.0164). Compared to λmax of N3 (proton)K+I_3^-, we conclude that the $K^+I_3^-$ aggregation to N3 is much more dramatic, causing favorable energy structure change of N3 (proton) followed by coordination geometry change.

5. Materials and Methods

The DFT-based MM with the SPARTAN'18 (Wavefunction, Inc. Irving, CA, USA) program code can be conducted by using high-end personal computers, deriving equilibrium geometries of van der Waals (vdW) aggregates such as I_2 and KI, and their aggregates with a Ru complex (N3 dye) and TiO_2 NP, along with the isosurface of the electrostatic potential based on the electronic charge distribution, thus helping us to gain insights into the nature of the iodine-based vdW bonds. Similar to the previous works [1–6], the DFT-based MM with B3LYP/6-31G(d) was employed to obtain the equilibrium geometry and electronic structure of vdW aggregates. Prior to the DFT calculation, the geometries of the molecular aggregates were determined by the molecular mechanics with the Merck molecular force field (MMFF) [21], so that the intermolecular vdW interaction and the electrostatic interaction was taken into account. The following calculation at the B3LYP/6-31G(d) level results in equilibrium geometry, van der Waals bonding is correctly described.

To simulate UV-Vis spectra revealing allowed electronic transitions with wavelength and intensity, we used the time-dependent DFT within the linear response regime [22,23]. The surface electron density and electrostatic potential map were used to elucidate molecular aggregation with vdW and electrostatic Coulomb interaction without covalent bonding. For a review of the quantum mechanical methods used in SPARTAN, see reference [24–27].

Supplementary Materials: The following are available online at http://www.mdpi.com/1996-1073/13/11/3027/s1, Figure S1: Energy structure of vdW-aggregate of N3 with acetonitrile (AN) of N3 and $(AN)_2$: UV/Vis spectrum and surface electron energy structure.

Author Contributions: Conceptualization, S.Y. (Susumu Yanagisawa) and S.Y. (Shozo Yanagida); methodology, software, validation and formal analysis, S.Y. (Shozo Yanagida); investigation, S.Y. (Susumu Yanagisawa) and S.Y. (Shozo Yanagida); resources, S.Y. (Shozo Yanagida); writing—original draft preparation, S.Y. (Susumu Yanagisawa); supervision, S.Y. (Shozo Yanagida); project administration, S.Y. (Shozo Yanagida); funding acquisition, S.Y. (Shozo Yanagida). All authors have read and agreed to the published version of the manuscript.

Funding: This research received no external funding.

Acknowledgments: The authors thank W. J. Hehre (Wavefunction, Inc. Irvine, CA, USA), and N. Uchida and Y. Watanabe (Wavefunction, Inc. Japan Branch Office, Kouji-machi, Chiyoda-ku, Tokyo Japan) for discussion on DFT-based molecular modeling using 'Spartan 19'.

Conflicts of Interest: The authors declare no conflict of interest.

Abbreviations

The following abbreviations are used in this manuscript:

vdW	van der Waals
MM	Molecular modelling
LUMO	Lowest-unoccupied molecular orbital
ESPM	Electrostatic potential map
MMFF	Merck molecular force field
DFT	Density functional theory
HOMO	Highest-occupied molecular orbital
DSSC	Dye-sensitized solar cell
NP	Nanoparticle

References

1. Yanagida, S.; Yanagisawa, S.; Segawa, H. Molecular Orbital-Based Verification of Conductivity of Tetramethylammonium Pentaiodide and Pentaiodide-Based Electrolytes in Dye-Sensitized Solar Cells. *J. Electrochem. Soc.* **2015**, *162*, E263–E270. [CrossRef]
2. Yanagida, S.; Yanagisawa, S.; Segawa, H. Computational Verification of So-Called Perovskite Solar Cells as PbI64−-Aligned Solar Cells. *J. Electrochem. Soc.* **2017**, *164*, E3598–E3605. [CrossRef]
3. Yanagida, S.; Yanagisawa, S.; Yanagida, M.; Segawa, H. Validity of density-functional-theory-based molecular modeling for UV/visible spectroscopy and rationale of panchromatic PbI6 4−(MeNH3+) 4-structured molecular solar cells. *Jpn. J. Appl. Phys.* **2018**, *57*, 121602. [CrossRef]
4. Yanagida, S.; Osabe, K.; Nagai, T.; Murakami, N. Quantum chemistry molecular modeling for longevity: Importance of antioxidative effects in mitochondria as battery of cells. *Integr. Mol. Med.* **2019**, *6*, 1–6. [CrossRef]
5. Yanagida, S.; Kaname, A.; Murakami, N. Quantum chemistry-based verification of antioxidative action of iodide in mitochondria. *Integr. Mol. Med.* **2019**, *6*, 1–6. [CrossRef]
6. Yanagida, S.; Yanagisawa, S.; Murakami, N. Quantum chemistry molecular modelling for mitochondria targeted chemotherapy: Verification of oxidative stress on mitochondria and anticancer medicines. *Integr. Mol. Med.* **2020**, *7*, 1–7. [CrossRef]
7. O'Regan, B.; Grätzel, M. A low-cost, high-efficiency solar cell based on dye-sensitized colloidal TiO_2 films. *Nature* **1991**, *353*, 737–740. [CrossRef]
8. Jiang, J.-K.; Yanagida, S. Optimization of Redox Mediators and Electrolysis. In *Dye-sensitized Solar Cells*; EPFL Press (Distributed by CRC Press): Lausanne, Switzerland, 2010; Chapter 4; pp. 117–144.
9. Xia, J.; Yanagida, S. Strategy to improve the performance of dye-sensitized solar cells: Interface engineering principle. *Sol. Energy* **2011**, *85*, 3143–3159. [CrossRef]
10. Zhang, S.; Yang, X.; Zhang, K.; Chen, H.; Yanagida, M.; Han, L. Effects of 4-tert-butylpyridine on the quasi-Fermi levels of TiO_2 films in the presence of different cations in dye-sensitized solar cells. *Phys. Chem. Chem. Phys.* **2011**, *13*, 19310–19313. [CrossRef] [PubMed]
11. Boschloo, G.; Haggman, L.; Hagfeldt, A. Quantification of the effect of 4-tert-butylpyridine addition to I-/I3-redox electrolytes in dye-sensitized nanostructured TiO_2 solar cells. *J. Phys. Chem. B* **2006**, *110*, 13144–13150. [CrossRef]
12. Zhang, S.; Yanagida, M.; Yang, X.; Han, L. Effect of 4-tert-butylpyridine on the quasi-Fermi level of dye-sensitized TiO_2 films. *Appl. Phys. Express* **2011**, *4*, 042301. [CrossRef]
13. Zhang, K.; Zhang, S.; Sodeyama, K.; Yang, X.; Chen, H.; Yanagida, M.; Tateyama, Y.; Han, L. A new factor affecting the performance of dye-sensitized solar cells in the presence of 4-tert-butylpyridine. *Appl. Phys. Express* **2012**, *5*, 042303. [CrossRef]
14. Jono, R.; Fujisawa, J.; Segawa, H.; Yamashita, K. Theoretical study of the surface complex between TiO_2 and TCNQ showing interfacial charge-transfer transitions. *J. Phys. Chem. Lett.* **2011**, *2*, 1167–1170. [CrossRef] [PubMed]
15. Yanagida, S.; Yanagisawa, S.; Yamashita, K.; Jono, R.; Segawa, H. Theoretical Verification of Photoelectrochemical Water Oxidation Using Nanocrystalline TiO_2 Electrodes. *Molecules* **2015**, *20*, 9732–9744. [CrossRef] [PubMed]
16. Yum, J.-H.; Nazzeeruddin, M.K. Molecular Engineering of Sensitizers for Conversion of Solar Energy into Electricity. In *Dye-sensitized Solar Cells*; EPFL Press (Distributed by CRC Press): Lausanne, Switzerland, 2010; Chapter 3; pp. 84–116.
17. Hagfeldt, A.; Boschloo, G.; Sun, L.; Kloo, L.; Pettersson, H. Dye-sensitized Solar Cells. *Chem. Rev.* **2010**, *110*, 6595–6663. [CrossRef] [PubMed]
18. Persson, P.; Lundqvist, M.J. Calculated structural and electronic interactions of the ruthenium dye N3 with a titanium dioxide nanocrystal. *J. Phys. Chem. B* **2005**, *109*, 11918–11924. [CrossRef] [PubMed]
19. Labat, F.; Ciofini, I.; Hratchian, H.P.; Frisch, M.J.; Raghavachari, K.; Adamo, C. Insights into working principles of ruthenium polypyridyl dye-sensitized solar cells from first principles modeling. *J. Phys. Chem. C* **2011**, *115*, 4297–4306. [CrossRef]
20. Angelis, F.D.; Fantacci, S. Theoretical and Model. System Calculation. In *Dye-Sensitized Solar Cells*; EPFL Press (Distributed by CRC Press): Lausanne, Switzerland, 2010; Chapter 13; pp. 555–591.

21. Küpper, F.C.; Feiters, M.C.; Olofsson, B.; Kaiho, T.; Yanagida, S.; Zimmermann, M.B.; Carpenter, L.J.; Luther, G.W., III; Lu, Z.; Jonsson, M.; et al. Commemorating Two Centuries of Iodine Research: An Interdisciplinary Overview of Current Research. *Angew. Chem. Int. Ed.* **2011**, *50*, 11598–11620. [CrossRef] [PubMed]
22. Roy, J.K.; Kar, S.; Leszczynski, J. Insight into the optoelectronic properties of designed solar cells efficient tetrahydroquinoline dye-sensitizers on TiO_2 (101) surface: First principles approach. *Sci. Rep.* **2018**, *8*, 10997. [CrossRef] [PubMed]
23. Zych, D.; Slodek, A. Sensitizers for DSSC containing triazole motif with acceptor/donor substituents—Correlation between theoretical and experimental data in prediction of consistent photophysical parameters. *J. Mol. Struct.* **2020**, *1207*, 127771. [CrossRef]
24. Halgren, A. Merck molecular force field. I. Basis, form, scope, parameterization, and performance of MMFF94. *J. Comput. Chem.* **1996**, *17*, 490. [CrossRef]
25. Burke, K.; Werschnik, J.; Gross, E.K.U. Time-dependent density functional theory: Past, present, and future. *J. Chem. Phys.* **2005**, *123*, 062206. [CrossRef] [PubMed]
26. Dreuw, A.; Head-Gordon, M. Single-reference ab initio methods for the calculation of excited states of large molecules. *Chem. Rev.* **2005**, *105*, 4009–4037. [CrossRef] [PubMed]
27. Shao, Y.; Molnar, L.F.; Jung, Y.; Kussmann, J.; Ochsenfeld, C.; Brown, S.T.; Gilbert, A.T.B.; Slipchenko, L.V.; Levchenko, S.V.; O'Neill, D.P.; et al. Advances in methods and algorithms in a modern quantum chemistry program package. *Phys. Chem. Chem. Phys.* **2006**, *8*, 3172–3191. [CrossRef] [PubMed]